Quench dynamics of stripes and phase separation in the two-dimensional t-J model

Luke Staszewski [*] and Alexander Wietek

Max Planck Institute for the Physics of Complex Systems, Nöthnitzer Straße 38, Dresden 01187, Germany

(Received 11 November 2024; revised 22 April 2025; accepted 29 May 2025; published 9 July 2025)

We investigate the fundamental dynamical process of an initial quench of the chemical potential of the two-dimensional t-J model. Depending on the ground-state phase, sharply different dynamical behaviors of the charge distribution and entanglement properties are observed. In the stripe phase, the intertwining of the spin and charge density waves remains stable under time evolution. A ballistic spreading of the charge density is observed with a propagation speed that is only weakly dependent on the coupling ratio J/t. Moreover, in the phase-separated regime for large J/t, we report a complete dynamical freezing of charge degrees of freedom within, where even under long time evolution the entanglement entropy remains bounded. Our results are obtained by combining large-scale exact-diagonalization and matrix-product-state techniques for time evolution.

DOI: 10.1103/nfmp-32tt

I. INTRODUCTION

Nonequilibrium dynamics can serve as a window to probing the intricate physics of strongly correlated quantum matter. While conventional transport measurements are often readily accessible in experiments, pump-probe experiments have recently yielded many insights into the physics of strongly correlated superconductors [1–3]. Moreover, ultracold atom experiments allow us to closely track the dynamics of individual atoms [4–7], and interesting dynamical processes, like quantum quenches [5,8] and Floquet dynamics [9], can be studied in unprecedented detail.

A particularly fascinating class of quantum materials comprises doped Mott insulators. While the high-temperature copper oxide superconductors are prime examples where doping a parent Mott insulator can induce superconductivity, we now know many more compounds exhibiting similar physics. This ranges from the transition metal dichalcogenides [10,11] to twisted moiré materials [12–17] and the nickelate superconductors [18,19]. From a theory perspective, the Hubbard model and the related t-J model [20–22] in two dimensions have been understood to capture the essential aspects of these complex phenomena—not without having posed significant challenges for both analytical and numerical studies [23,24]. Modern developments in numerical algorithms have led to rather firm insights concerning the ground state [25–31] as well as finite-temperature properties [32–34]. Currently, nonequilibrium properties of these models are at the forefront of computational and theoretical research.

Early on, the dynamics of strongly correlated fermionic and bosonic systems was studied intensely in one spatial dimension [35–37], where analytical techniques, such as the Bethe ansatz, as well as numerical techniques are both readily available. The authors of these studies revealed that nonthermal steady states which strongly depend on the initial condition can be realized after a quench in the system parameters.

A major open question concerns the electronic transport in strongly correlated electron systems. Fundamentally, an understanding is still lacking of how individual charge carriers are able to spread throughout strongly correlated phases, such as stripes, superconductors, and phase separated regimes, all observed within the cuprate superconductors. Here, we explore the question of how a nonuniform charge distribution evolves in an isolated closed system, throughout different correlated phases in the t-J model. We consider this numerical experiment as an important step toward understanding more intricate transport properties. A nonuniform charge distribution can experimentally be realized by gate voltages in a material compound or by varying the local chemical potential in an ultracold atom experiment. Scanning

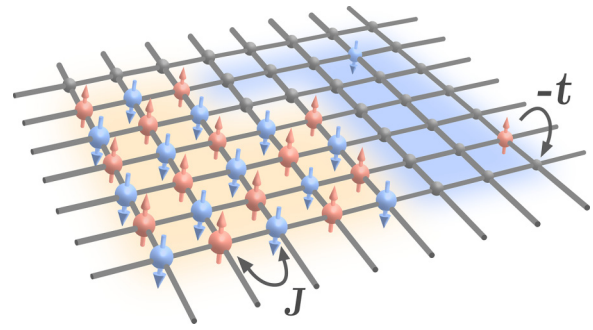

FIG. 1. Initial setup of quench in the t-J model. We perform an inhomogeneous quench of the chemical potential in the t-J model. The initial state has one half of the system having one electron per site with antiferromagnetic correlations and the other half with a lower electron density. Phase separation in the model leads to this initial state being dynamically frozen for large J/t.

[*] Contact author: lstaszewski@pks.mpg.de

Published by the American Physical Society under the terms of the Creative Commons Attribution 4.0 International license. Further distribution of this work must maintain attribution to the author(s) and the published article's title, journal citation, and DOI. Open access publication funded by Max Planck Society.

tunneling microscopy experiments can accurately map the charge distribution in two-dimensional planes, for example, in high-temperature superconductors where charge density waves, stripes, and phase separated regions have been observed [38–41]. For these measurements to be possible, the charge distribution is required to fluctuate little on the timescale of the experiment. Charge dynamics are also tightly bound to transport coefficients, which give key signatures of metallic, insulating, and superconducting behavior. Thus, a detailed understanding of the charge dynamics in interacting electron systems is highly sought after. This applies especially for strange metal and pseudogap regimes, where clustering and forestalled phase separation of charges has been recently reported; the precise implications on transport are yet to be understood [42].

In two spatial dimensions, authors of several studies have considered the dynamics of a single hole in a Mott insulating background [43–45]. Ultracold atoms have been used to actively study both the dynamics of mobile holes in an antiferromagnetic background [46–48] as well as bad metallic transport by analyzing the dynamical relaxation of an imposed density modulation [7]. Mobility constraints, i.e., dynamical freezing arising from dipole conservation laws and fractonlike physics, have also drawn theoretical interest to the subject [49–52].

In this study, we use a combination of exact diagonalization (ED) using Lanczos techniques on system sizes of up to 28 sites as well as the time-dependent variational principle (TDVP) method for matrix product states (MPSs)on system sizes of up to 64 sites to establish the dynamical properties of the t-J model subject to an inhomogeneous quench in the chemical potential, see Fig. 1. Our findings show that a quench for large J/t leads to a completely frozen dynamical regime. We also demonstrate that a quench for $J/t \sim 0.4$ leads to coherent oscillations of stripes for long times. Lastly, we see that small J/t leads to regions of ferromagnetic and antiferromagnetic correlations that remain remarkably stable adjacent to one another.

II. MODEL

The Hamiltonian for the t-J model is given by

$$H = -t \sum_{\langle i,j\rangle,\sigma} (\tilde{c}^{\dagger}_{i,\sigma}\tilde{c}_{j,\sigma} + \text{H.c.}) + J \sum_{\langle i,j\rangle} \left(\mathbf{S}_i \cdot \mathbf{S}_j - \frac{n_i n_j}{4}\right), \quad (1)$$

where the operators $\tilde{c}^{\dagger}_{i,\sigma}$ are electron creation operators of spin $\sigma = \uparrow, \downarrow$ at site i that project onto single-site occupancies, thereby forbidding doubly occupied sites in the model. Here, $\langle i, j\rangle$ denotes summation over nearest neighbors on a square lattice, $\mathbf{S}_i = (S^x_i, S^y_i, S^z_i)^T$ are electron spin operators, and n_i is the number operator on site i.

We study the model in the absence of next-nearest-neighbor hopping, where there is no expected pairing in the ground-state wave function [53–55]. We show an approximate phase diagram in Fig. 2(a) at a doping of $\frac{1}{8}$ obtained through density matrix renormalization group (DMRG) calculations; a more detailed discussion of the phase diagram is given in Appendix A.

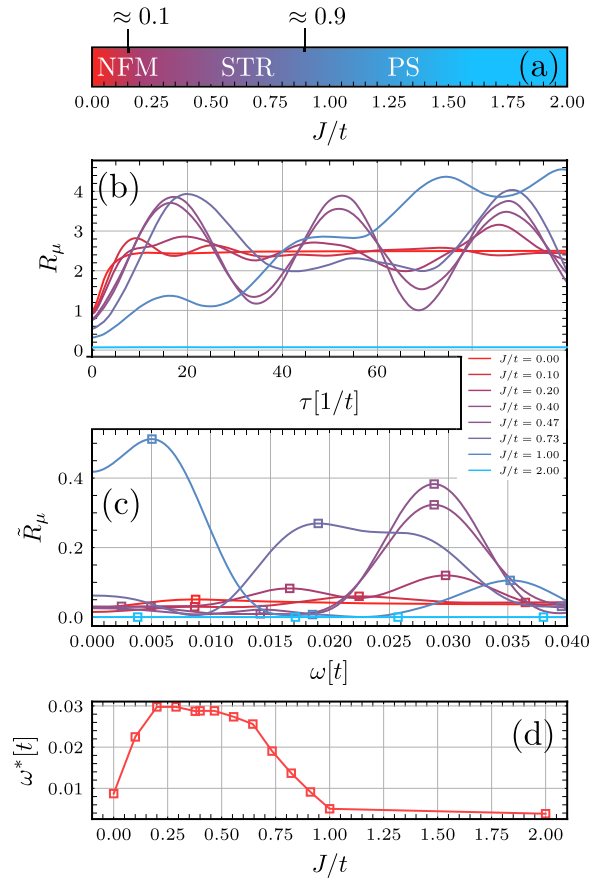

FIG. 2. Phase diagram and center of mass evolution. (a) We compute a phase diagram at zero temperature for the 2D t-J model at a doping of 0.125 by using DMRG on a 16×4 cylindrical geometry. (b) ED time evolution of two holes on a 6×4 site cluster. We show the center of mass of the two holes R_μ following a quench [see the thick red line of Fig. 3(a)]. (c) We compute the Fourier transform $\tilde{R}_\mu$ of the center of mass data from (b) to analyze the frequency of the coherent oscillations and the corresponding hole speed in the striped phase. (d) Dominant frequency ω^* for each J/t. We note a relatively weak dependence on the speed of the two holes throughout the striped phase.

III. TIME EVOLUTION

We use two computational methods to analyze the real space and time dynamics of holes on a square lattice governed by the t-J model—ED and MPS. In what follows, we study a cylindrical geometry where periodic (open) boundary conditions are employed along the shorter (longer) direction of the lattice. We also introduce a natural notion of left and right into the system, by partitioning the sites with a cut perpendicular to the axis of the cylinder. Times are denoted by τ in all plots and given in units of the inverse tunneling amplitude $1/t$.

The initial state for the time evolution is obtained by applying a large chemical potential $\mu = 100t$ to the right half of the system and finding the ground-state wave function. We choose an overall hole doping of $p = \frac{1}{16}$, which effectively

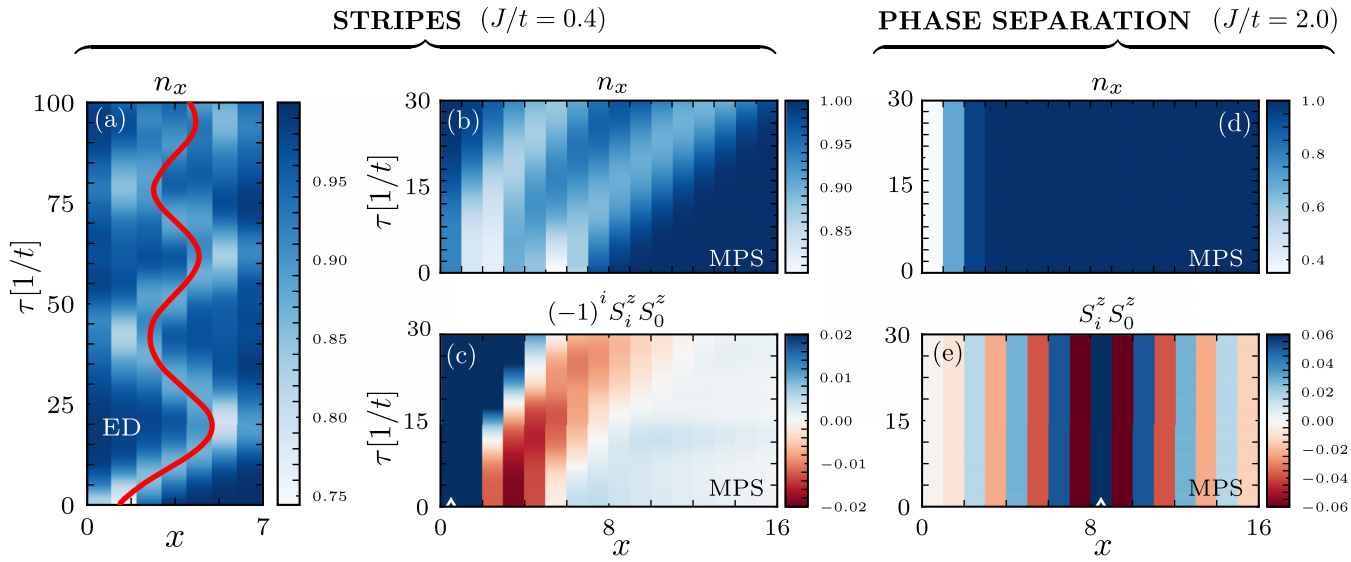

FIG. 3. Dynamics of stripes and phase separation in the t-J model. (a) We use ED to compute the rung density n_x (outlined in the main text) of two holes on a 7×4 site lattice, subject to a quench of the chemical potential for $J/t = 0.4$. We observe long-lived coherent oscillations. (b) and (c) Rung density and staggered spin correlations for the same quench at $J/t = 0.4$, with an MPS simulation on a 16×4 site lattice with four holes. Stripes formed on the left half of the system ballistically spread toward the right side of the system. (d) and (e) Rung density and spin correlations for an MPS simulation of the quench with $J/t = 2.0$. The initial phase-separated state with holes on one half of the system remains frozen.

translates to a doping of $p = \frac{1}{8}$ on the left half of system. With ED, this is performed using Lanczos, while for larger systems with MPSs, we use the DMRG technique. The system is then quenched by switching off this potential and allowing the holes to evolve under the Hamiltonian of Sec. 1. We consider the rung density $n_x = \frac{1}{L_y}\sum_y n_{x,y}$ as well as spin correlations, shown in Fig. 3 for several quenches.

We follow Expokit's Krylov-based method [56] in time evolving the initial state—working to within a global error of 10^{-8} using a Krylov subspace dimension size between 10 and 30. Figure 3(a) shows the time evolution of the rung density for a 7×4 site ED calculation for $J/t = 0.4$.

To perform time evolution on larger system sizes, we use the two-site TDVP algorithm [57,58] and work down to a truncation error of 10^{-7}. Here, the time evolution is limited by the growth of entanglement entropy. The rung density for a simulation on a 16×4 site cylinder is presented for $J/t = 0.4$ and 2.0 in Figs. 3(b) and 3(c), respectively. The former case shows a coherent motion of the hole density up to the simulated times of $\tau = 30/t$. We observe this coherent motion for much longer times in the ED calculation of Fig. 3(a). The behavior for larger J/t is a completely frozen regime in which the holes remain pinned to one half of the system. Both the ED and MPS simulations could be carried out up to $\tau = 100/t$ showing no spreading of the hole density.

From the rung density, we then compute the center of mass of the holes during the evolution

$$R_\mu = \frac{L_y}{N_h}\sum_x x(1 - n_x). \tag{2}$$

where N_h is the total number of holes, and R_μ is shown with a red line in Fig. 3(a) and for several values of J/t in Fig. 2(b).

This time evolution indicates a series of interesting dynamical regimes of the t-J model, which we will now proceed to discuss in the context of the ground-state phase diagram. We leave a discussion of the convergence of the TDVP results to Appendix B.

IV. THREE DYNAMICAL REGIMES

Performing DMRG on a width-four cylinder at doping of $p = \frac{1}{8}$ reveals three phases as we vary the magnetic coupling J/t—a phase-separated state for $J/t > 0.92$, a stripe phase for $0.10 < J/t < 0.92$, and an insulating Nagaoka ferromagnet (NFM) when $J/t < 0.10$—Fig. 2(a).

Our ED calculations in Fig. 2(b) indicate that each of these phases is accompanied by a distinctive dynamical regime in performing the quench outlined from Sec. III. In this section, we combine the longer ED time evolution with that of MPS simulations on larger system sizes and discuss the corresponding dynamics for each of these phases in turn.

A. Stripes

We first discuss intermediate values of $J/t \sim 0.4$ relevant to the cuprates, for which we observe a wide range of magnetic couplings where stripes prevail. Stripes were predicted by Hartree-Fock solutions to the Hubbard model [59–61]. They describe a situation in which the holes situate on the boundary of an antiferromagnetic domain wall. From our time evolution, we observe the hole density of the stripes to be ballistic in nature up to the times we were able to simulate. For the ED where just two holes are present, the two holes remain locally bound together and oscillate back and forth, reflecting off of the boundary of the cylinder, Fig. 3(a).

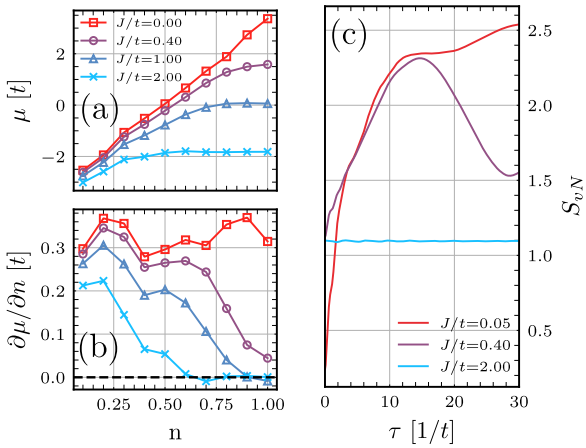

FIG. 4. Maxwell construction and growth of von Neumann entropy. (a) We compute the ground-state energy using ED as a function of filling n. (b) Derivative of μ with respect to n, which vanishes when phase separation occurs. (c) Growth of the of the von Neumann entropy S_{vN} computed during the MPS time evolution. In the phase-separated case, we note that there is no growth in the von Neumann entropy.

Larger system sizes also indicate a ballistic nature to the motion for the hole density following the quench. An initial state (in the presence of a chemical potential) realizes two stripes on one half of the system. These high hole-density regions remain stable and spread across the system without mixing for the timescales simulated in Fig. 3(b). The domain walls of the antiferromagnet can be seen to track the maxima of the hole density as they spread by looking at the staggered spin correlations shown in Fig. 3(c).

We find the speed at which the holes move and the stripes spread has only a very weak dependency on the magnetic coupling J/t. This is seen from the ED time evolution of Fig. 2, in which we first compute the center of mass of the hole density for two holes on a 6×4 cluster R_μ and take the dominant frequency ω^* from the Fourier transformed data (d). We find this frequency ω^* to be relatively constant throughout the striped phase and see the onset of a dominant low-frequency peak as J/t is increased toward the onset of phase separation.

B. Phase separation

Once J/t is large enough, we cross over from a striped phase into phase separation. Early researchers into the Hubbard and t-J models raised the question of phase separation and its role in the cuprates. While phase coexistence was not found at parameters relevant to the cuprates, it is present in the t-J model and has a strong consequence for the dynamics. We establish phase separation in the t-J model at a doping of $p = \frac{1}{8}$ for $J/t > 1$ by means of a Maxwell construction. Using ED calculations on 20 sites, we obtain the chemical potential μ for different fillings n at zero temperature, Fig. 4(a). Regions of constant chemical potential show the onset of phase coexistence for $J/t > 1$. Phase separation is also supported with DMRG calculations on larger system sizes with the aforementioned geometry by computing the charge structure factor and analyzing the charge density, which we leave to Appendix A.

The phase separation has an extremely strong consequence for the dynamics following the quench we performed—it results in a completely frozen dynamical regime. The rung density, shown in Fig. 3(d), is static for the duration of the calculated time evolution. This persists even up to times of $100/t$ where the long time evolution is possible due to a lack of entanglement growth Fig. 4(c). The holes remain bound to the one half of the system from which they started, failing to mix with the antiferromagnet for all times we were able to simulate due to the phase coexisting ground state tending toward a mutual eigenstate of the system in the presence of a chemical potential imbalance.

C. Nagaoka ferromagnetism

The final dynamical regime we would like to discuss lies in the region of small $J/t < 0.1$ of the phase diagram in Fig. 2(a). A theorem due to Nagaoka predicts that a single-hole-doped Hubbard model with infinite repulsive interaction (corresponding to $J/t = 0$ in the t-J model) admits an itinerant ferromagnetic ground state [62] and has attracted attention recently in an out-of-equilibrium context [63,64]. We observe the onset of ferromagnetic correlation in the DMRG simulations with domains of length two. This leads to the interesting initial state of our quench presenting the interface between a Nagaoka ferromagnet and a Mott antiferromagnet. While our ED calculations demonstrate a fast approach to equilibrium in this regime, the absence of ferromagnetic correlation on the small system size leads to a contrast with what we see from the TDVP simulations. Here, we observe that the ferromagnetic correlations are extremely slow to mix with the antiferromagnetically correlated half of the cylinder and a very slow spreading of the charge degrees of freedom due to the insulating nature of both phases. We therefore leave the MPS time evolution for $J/t = 0.05$ in Fig. 5.

V. DISCUSSION AND CONCLUSIONS

In this work, we have investigated the real-time, real-space quench dynamics of a model paradigmatic to the study of strongly correlated electrons. We have shown using a combination of ED and MPS calculations that a quench in the chemical potential of the t-J model can lead to several interesting dynamical regimes. For $J/t \sim 0.4$, where the ground state shows stripes, we observe long-lived coherent oscillations of these stripes. We find that the speed at which the stripe spreads has a relatively weak dependence on the magnetic coupling J. Ultimately, we expect for long enough times a thermalization, which happens at longer timescales beyond that simulated.

We have shown that large J/t, where the ground state is phase separated, leads to a complete freezing in the dynamics. Here, there is no growth in entanglement due to the freezing, and the initial hole-rich region remains pinned to one half of the system. Lastly, we find that, for small J/t, while the hole-dense region seems to rapidly mix with the antiferromagnetic insulating region on small systems, for large systems, where we start to observe the onset of ferromagnetic correlations,

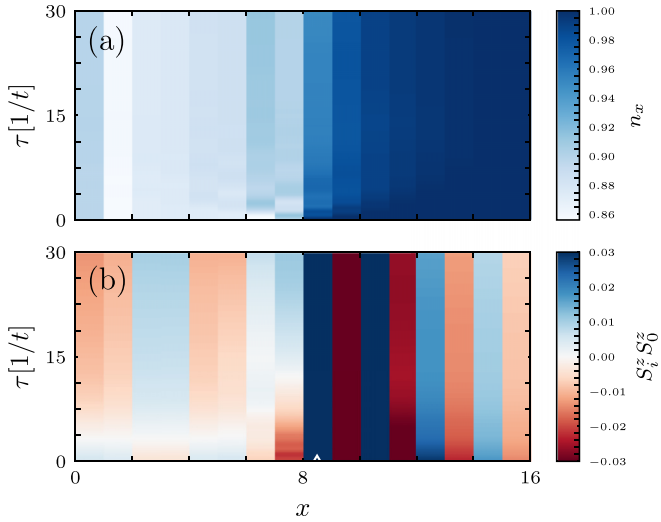

FIG. 5. Dynamics of the Nagaoka ferromagnet. Rung density and spin correlations for a quench of the chemical potential for $J/t = 0.05$. On the hole-doped side of the cylinder (left), ferromagnetic correlations arise.

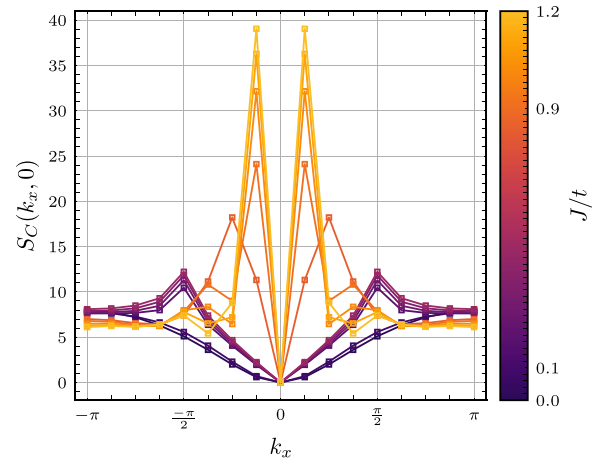

FIG. 6. Charge structure from DMRG. We calculate the charge structure factor at $k_y = 0$ from the ground state obtained using DMRG on a 16×4 site cylinder. We work down to a truncation error of $<10^{-5}$ and identify three phases: a commensurate checkerboard insulator, a striped phase, and phase separation. We combine this with spin-structure factor, hole-density distribution, and Maxwell construction to estimate the phase boundaries indicated in Fig. 2.

this mixing seems to become inhibited, and we leave the precise characterization of the dynamics in this regime to future studies due to the large sensitivity of the time evolution to exact doping and J/t.

Our results lay a foundation for understanding transport in the type of electron phases encountered in strongly correlated superconductors. The stability of nonuniform charge distributions is particularly relevant to understand scanning tunneling microscopy experiments, where charge distributions are required to remain stable on the timescale of the experiment. Recent results [42] point toward a clustering and phase-separation instability in the two-dimensional Hubbard model in the pseudogap regime. As we have demonstrated, phase separation leads to a complete dynamical freezing which in turn could be related to the large resistivity encountered in cuprates in the pseudogap and strange and bad metal regimes. Moreover, nonequilibrium properties of Fermi Hubbard models can be readily probed using ultracold atoms at intermediate temperatures [4–7]. Cold atom setups are now able to achieve low enough temperatures to probe pseudogap physics, and it is not inconceivable that the physics of stripe correlations are also soon to be within reach [65,66]. As nonequilibrium questions can readily be probed in quantum simulators [7], our findings constitute the basis of understanding dynamical properties of nonuniform charge distributions in strongly correlated electrons, which can be further corroborated by more elaborate experiments.

ACKNOWLEDGMENTS

We thank Salvatore Manmana, John Sous, Aritra Sinha, Martin Ulaga, and Roderich Moessner for insightful discussions. A.W. acknowledges support by the German Research Foundation (DFG) through the Emmy Noether program (Grant No. 509755282). The ED simulations were performed using the XDiag library [67]. The DMRG and TDVP simulations have been performed using the Julia version of the ITensor library [68,69].

APPENDIX A: PHASE DIAGRAM

In order to identify the phases present in the t-J model at a doping of 0.125 we use DMRG, retaining up to 2000 states and performing 200 sweeps. We measure local electron density $n(x, y)$ as well as density and spin correlations. We then extract the approximate phase boundary for the transition from a Nagaoka ferromagnet to a striped phase at $J/t \sim 0.1$ by noting a jump in the charge structure factor (see Fig. 6). The charge structure factor shows a quadratic dispersion at low momenta for $J/t < 0.1$, which becomes linear for $J/t > 0$, suggesting the closing of a charge gap. For the $J/t > 0.1$ there is also a clear peak in the charge structure factor at a momentum $\pi/2$ due to the wavelength four charge density wave. Figure 7(b) also shows the charge density and spin correlation on the width four cylinders, which demonstrates the antiferromagnetic correlations with domain walls at the hole maxima-characteristic of a stripe.

The boundary for the transition, from stripes to phase separation is also seen in the charge structure factor, but less clear. Once the peak swaps to the lowest non-zero momentum, the charge density is modulated on a length scale that increases with system size [seen in Fig. 7(a)] and the hole density is forced to the edge of the cylinder. This is phase separation between a region of zero hole density [center of the cylinder in Fig. 7(a)] with strong antiferromagnetic correlations and a high hole density region at the edge of the cylinder. We supplement establishing the boundary of the onset of phase separation by using DMRG at different dopings to perform a Maxwell construction (as in Fig. 4) and find that the onset of phase separation is for $J/t \sim 1$ on the width four cylinder.

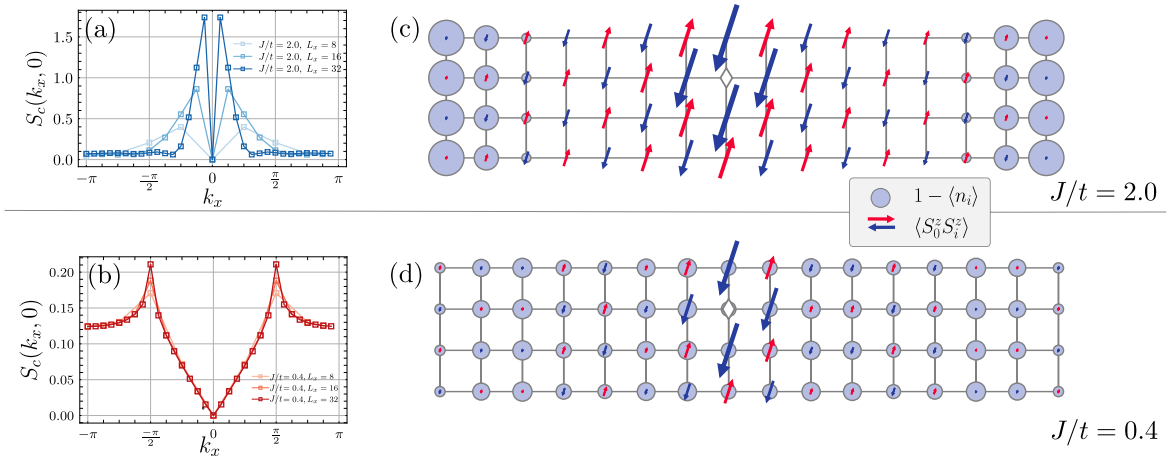

FIG. 7. Phase separation and stripes in the t-J model. Charge structure factor at $k_y = 0$ calculated with DMRG for (a) $J/t = 2.0$ and (b) $J/t = 0.4$. From light to dark shows increasing system size (length of the cylinder). For $J/t = 2.0$ (blue), a peak forms at the inner-most nonzero value of k_x. This is indicative of phase separation. (b) shows the formation of a peak at $k_x = \pi/4$ due to a charge density wave. Hole density profile and spin correlations for the ground state from DMRG for (c) $J/t = 2.0$ and (d) $J/t = 0.4$. The white diamond marks the reference site for the spin correlations. For the phase-separated case, we note that the holes form at the edge of the cylinder, in contrast with the striped phase where a minimum in the hole density is observed at the boundary.

APPENDIX B: CONVERGENCE OF RESULTS

The MPS approximation to the true time evolved wave function becomes a poorer approximation due to the growth of entanglement. For the phase separated case convergence is not an issue, due to lack of growth in von Neumann entropy, whilst for the striped phase there is growth of entanglement. We are however, still able to time evolve with converged results up to times $30\frac{1}{t}$. We check for convergence in two ways. We first check that the bond dimension of the initial state (found with DMRG) does not affect the time evolution. We then check for a given bond dimension of the initial state that as we decrease the truncation error in the two site TDVP that the local electron density converges. This is shown in Fig. 8, where on several sites across the cylinder we check that the density is converged by computing the time evolution down to a truncation error of 10^{-7}.

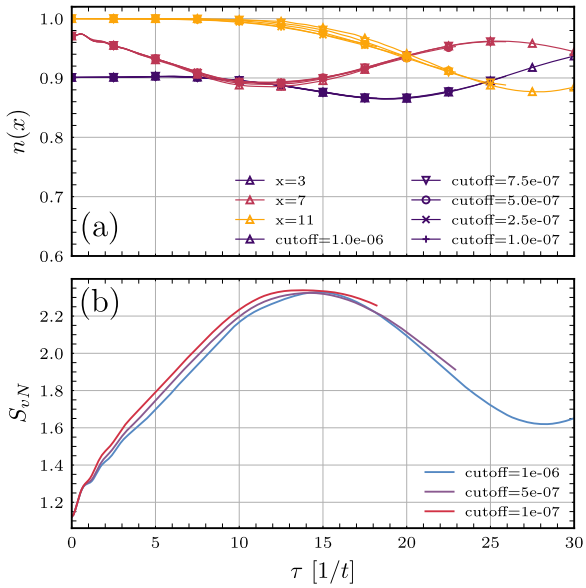

FIG. 8. Convergence of TDVP $J/t = 0.4$. (a) The on-site electron density as a function of time is calculated for cutoffs down to 10^{-7} for the TDVP time evolution used in Fig. 3(c). A bond dimension of 1000 was used to find the initial state, and a maximal bond dimension of 2000 was used for the time evolution of the MPS. (b) The entanglement entropy plotted for cutoffs from 10^{-6} down to 10^{-7}.

APPENDIX C: ROBUSTNESS OF THE QUENCH

We perform several checks to see how robust our results are to the specifics of the quench. These checks include, performing the time evolution on different cluster geometries,

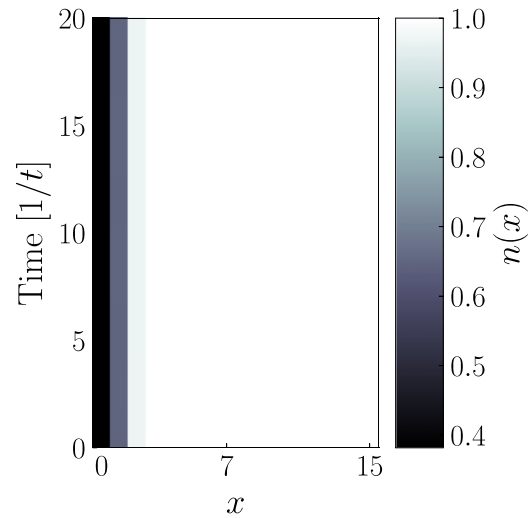

FIG. 9. Time evolution on a 16×6 cylinder. Freezing persists within the phase-separated region of the phase diagram ($J = 2.0t$) on this larger system size. Plotted is the rung density as a function of time, following the same quench outlined in the main text.

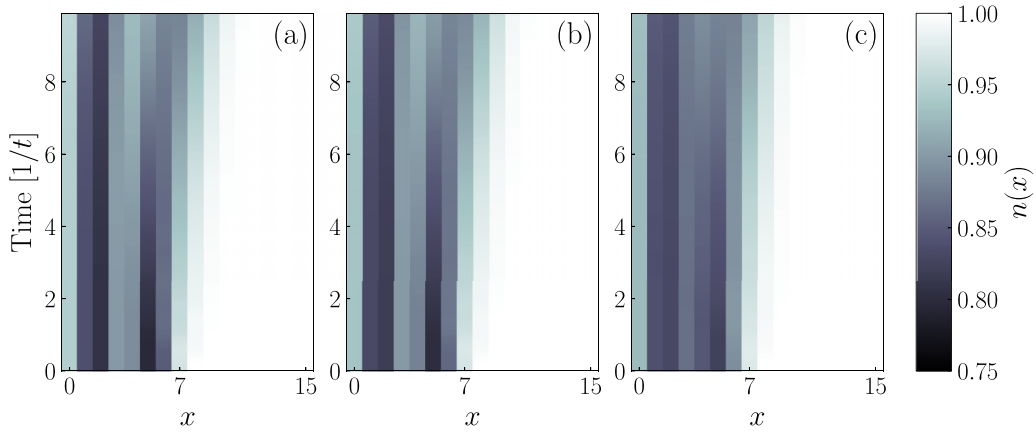

FIG. 10. Effect of longer range hopping. Time evolution of the rung density following the quench outlined in the main text for $J/t = 0.4$ as the next-nearest-neighbor hopping t'/t is varied -0.2, 0.0, and 0.2 from left to right. A negative t'/t seems to have very little effect on the resulting evolution of the charge density, while a positive t'/t leads to a qualitative difference and an apparent mixing of the two stripes.

different strengths of the chemical potential for the initial state preparation and we investigate the affect of longer range hopping on the real space dynamics of the t-J model.

In studying the quench dynamics of the two dimensional t-J model, we are limited to finite size clusters for this study. This has included time evolution using exact diagonalization on system size of 6×4, and we have seen that many of the effects observed on this relatively small yet exact study persist on larger system sizes when switching to an MPS representation of the wave function and performing the time evolution on system sizes up to 16×4 cylindrical geometries. In going to larger system sizes, this remains a serious numerical challenge. Whilst the initial state can be obtained on wider cylinder geometries, using DMRG, this requires significant bond dimensions which make the subsequent time evolution unfeasible, due to the further growth in entanglement. However, for the special case of $J/t = 2.0$, where we observe no growth in entanglement we are able to perform the time evolution on up to width 6 cylinder geometries, where we again see that freezing persists. Figure 9 shows the frozen charge density during the time evolution on a 16×6 cylinder geometry.

Another important question is how fine tuned the results of this study are. Figure 10 shows how the time evolution of the rung density on a 16×4 cylinder geometry is affected by the inclusion of longer range hopping. A small negative t'/t (hole doped) has no significant impact on the either the initial state charge density or the subsequent time evolution, where the stripes are observed to spread without mixing with each other, as in the case presented in the main text in the absence of such hopping terms. However, for the inclusion of a positive t'/t (the electron doped case), we observe a deviation from the former case, whereby the stripes appear to mix with each other. This coincides with the observed onset of superconductivity in the electron doped t-t'-J model, from previous DMRG studies [53].

We also assess what strength of chemical potential imbalance is required for the quench to produce the observed effects. For the case of $J/t = 0.4$, Fig. 11 shows the same

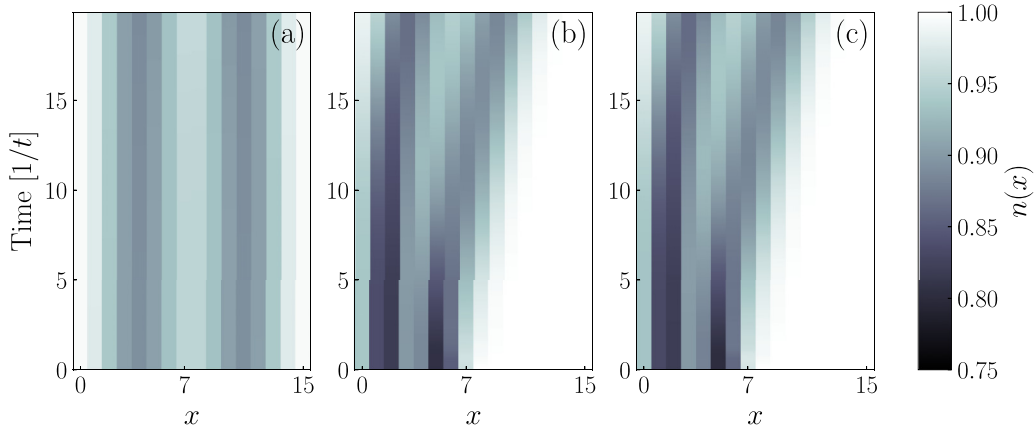

FIG. 11. Effect of chemical potential on the quench dynamics. We perform the time evolution outlined in the main text with different chemical potential and observe a robustness of the resulting dynamics to the strength of the chemical potential. μ/t (the initial chemical potential) is varied from 0, 10, and 100 (left to right). (a) For $\mu = 0$, the quenched Hamiltonian is the same as the initial one, hence time evolving the ground state. Once $\mu/t > 10$, we see no effects of further increasing the strength of the chemical potential.

quench with the chemical potential, μ/t varied from 0 to 100. We see that once $\mu/t > 10$ there are no further qualitative effects on the subsequent time evolution. We see similar behavior for other values of J/t and expect for the phase separated case, an arbitrarily small chemical potential should be required to see the observed freezing, though obtaining the initial state becomes increasingly difficult, due to the complex energy landscape.

[1] M.-A. Méasson, Y. Gallais, M. Cazayous, B. Clair, P. Rodière, L. Cario, and A. Sacuto, Amplitude Higgs mode in the $2H$-$NbSe_2$ superconductor, Phys. Rev. B **89**, 060503(R) (2014).

[2] B. Liu, M. Först, M. Fechner, D. Nicoletti, J. Porras, T. Loew, B. Keimer, and A. Cavalleri, Pump frequency resonances for light-induced incipient superconductivity in $YBa_2Cu_3O_{6.5}$, Phys. Rev. X **10**, 011053 (2020).

[3] S. J. Zhang, X. Y. Zhou, S. X. Xu, Q. Wu, L. Yue, Q. M. Liu, T. C. Hu, R. S. Li, J. Y. Yuan, C. C. Homes *et al.*, Light-induced melting of competing stripe orders without introducing superconductivity in $La_{2-x}Ba_xCuO_4$, Phys. Rev. X **14**, 011036 (2024).

[4] U. Schneider, L. Hackermüller, J. P. Ronzheimer, S. Will, S. Braun, T. Best, I. Bloch, E. Demler, S. Mandt, D. Rasch *et al.*, Fermionic transport and out-of-equilibrium dynamics in a homogeneous Hubbard model with ultracold atoms, Nat. Phys. **8**, 213 (2012).

[5] T. Langen, R. Geiger, and J. Schmiedmayer, Ultracold atoms out of equilibrium, Annu. Rev. Condens. Matter Phys. **6**, 201 (2015).

[6] S. Scherg, T. Kohlert, J. Herbrych, J. Stolpp, P. Bordia, U. Schneider, F. Heidrich-Meisner, I. Bloch, and M. Aidelsburger, Nonequilibrium mass transport in the 1D Fermi-Hubbard model, Phys. Rev. Lett. **121**, 130402 (2018).

[7] P. T. Brown, D. Mitra, E. Guardado-Sanchez, R. Nourafkan, A. Reymbaut, C.-D. Hébert, S. Bergeron, A.-M. S. Tremblay, J. Kokalj, D. A. Huse *et al.*, Bad metallic transport in a cold atom Fermi-Hubbard system, Science **363**, 379 (2019).

[8] A. Mitra, Quantum quench dynamics, Annu. Rev. Condens. Matter Phys. **9**, 245 (2018).

[9] M. Bukov, L. D'Alessio, and A. Polkovnikov, Universal high-frequency behavior of periodically driven systems: From dynamical stabilization to Floquet engineering, Adv. Phys. **64**, 139 (2015).

[10] W. Shi, J. Ye, Y. Zhang, R. Suzuki, M. Yoshida, J. Miyazaki, N. Inoue, Y. Saito, and Y. Iwasa, Superconductivity series in transition metal dichalcogenides by ionic gating, Sci. Rep. **5**, (2015).

[11] S. Manzeli, D. Ovchinnikov, D. Pasquier, O. V. Yazyev, and A. Kis, 2D transition metal dichalcogenides, Nat. Rev. Mater. **2**, 17033 (2017).

[12] Y. Cao, V. Fatemi, S. Fang, K. Watanabe, T. Taniguchi, E. Kaxiras, and P. Jarillo-Herrero, Unconventional superconductivity in magic-angle graphene superlattices, Nature (London) **556**, 43 (2018).

[13] M. Yankowitz, S. Chen, H. Polshyn, Y. Zhang, K. Watanabe, T. Taniguchi, D. Graf, A. F. Young, and C. R. Dean, Tuning superconductivity in twisted bilayer graphene, Science **363**, 1059 (2019).

[14] Y. Tang, L. Li, T. Li, Y. Xu, S. Liu, K. Barmak, K. Watanabe, T. Taniguchi, A. H. MacDonald, J. Shan *et al.*, Simulation of Hubbard model physics in WSe_2/WS_2 moiré superlattices, Nature (London) **579**, 353 (2020).

[15] L. Wang, E.-M. Shih, A. Ghiotto, L. Xian, D. A. Rhodes, C. Tan, M. Claassen, D. M. Kennes, Y. Bai, B. Kim *et al.*, Correlated electronic phases in twisted bilayer transition metal dichalcogenides, Nat. Mater. **19**, 861 (2020).

[16] T. Li, S. Jiang, L. Li, Y. Zhang, K. Kang, J. Zhu, K. Watanabe, T. Taniguchi, D. Chowdhury, L. Fu *et al.*, Continuous Mott transition in semiconductor moiré superlattices, Nature (London) **597**, 350 (2021).

[17] A. Ghiotto, E.-M. Shih, G. S. S. G. Pereira, D. A. Rhodes, B. Kim, J. Zang, A. J. Millis, K. Watanabe, T. Taniguchi, J. C. Hone *et al.*, Quantum criticality in twisted transition metal dichalcogenides, Nature (London) **597**, 345 (2021).

[18] D. Li, K. Lee, B. Y. Wang, M. Osada, S. Crossley, H. R. Lee, Y. Cui, Y. Hikita, and H. Y. Hwang, Superconductivity in an infinite-layer nickelate, Nature (London) **572**, 624 (2019).

[19] B. Y. Wang, K. Lee, and B. H. Goodge, Experimental progress in superconducting nickelates, Annu. Rev. Condens. Matter Phys. **15**, 305 (2024).

[20] P. W. Anderson, The resonating valence bond state in La_2CuO_4 and superconductivity, Science **235**, 1196 (1987).

[21] F. C. Zhang and T. M. Rice, Effective Hamiltonian for the superconducting Cu oxides, Phys. Rev. B **37**, 3759 (1988).

[22] V. J. Emery and G. Reiter, Mechanism for high-temperature superconductivity, Phys. Rev. B **38**, 4547 (1988).

[23] M. Qin, T. Schäfer, S. Andergassen, P. Corboz, and E. Gull, The Hubbard model: A computational perspective, Annu. Rev. Condens. Matter Phys. **13**, 275 (2022).

[24] D. P. Arovas, E. Berg, S. A. Kivelson, and S. Raghu, The Hubbard model, Annu. Rev. Condens. Matter Phys. **13**, 239 (2022).

[25] J. P. F. LeBlanc *et al.*, Solutions of the two-dimensional Hubbard model: Benchmarks and results from a wide range of numerical algorithms, Phys. Rev. X **5**, 041041 (2015).

[26] B.-X. Zheng, C.-M. Chung, P. Corboz, G. Ehlers, M.-P. Qin, R. M. Noack, H. Shi, S. R. White, S. Zhang, and G. K.-L. Chan, Stripe order in the underdoped region of the two-dimensional Hubbard model, Science **358**, 1155 (2017).

[27] M. Qin, C.-M. Chung, H. Shi, E. Vitali, C. Hubig, U. Schollwöck, S. R. White, and S. Zhang(Simons Collaboration on the Many-Electron Problem), Absence of superconductivity in the pure two-dimensional Hubbard model, Phys. Rev. X **10**, 031016 (2020).

[28] E. W. Huang, C. B. Mendl, S. Liu, S. Johnston, H.-C. Jiang, B. Moritz, and T. P. Devereaux, Numerical evidence of fluctuating stripes in the normal state of high-T_c cuprate superconductors, Science **358**, 1161 (2017).

[29] E. W. Huang, C. B. Mendl, H.-C. Jiang, B. Moritz, and T. P. Devereaux, Stripe order from the perspective of the Hubbard model, npj Quantum Mater. **3**, 22 (2018).

[30] A. Wietek, Fragmented cooper pair condensation in striped superconductors, Phys. Rev. Lett. **129**, 177001 (2022).

[31] N. Baldelli, B. Kloss, M. Fishman, and A. Wietek, Fragmented superconductivity in the Hubbard model as solitons in Ginzburg-Landau theory, arXiv:2307.11820.

[32] A. Wietek, Y.-Y. He, S. R. White, A. Georges, and E. M. Stoudenmire, Stripes, antiferromagnetism, and the pseudogap in the doped Hubbard model at finite temperature, Phys. Rev. X **11**, 031007 (2021).

[33] A. Wietek, R. Rossi, F. Šimkovic, M. Klett, P. Hansmann, M. Ferrero, E. M. Stoudenmire, T. Schäfer, and A. Georges, Mott insulating states with competing orders in the triangular lattice Hubbard model, Phys. Rev. X **11**, 041013 (2021).

[34] T. Schäfer *et al.*, Tracking the footprints of spin fluctuations: A multimethod, multimessenger study of the two-dimensional Hubbard model, Phys. Rev. X **11**, 011058 (2021).

[35] S. R. Manmana, S. Wessel, R. M. Noack, and A. Muramatsu, Strongly correlated fermions after a quantum quench, Phys. Rev. Lett. **98**, 210405 (2007).

[36] C. Kollath, A. M. Läuchli, and E. Altman, Quench dynamics and nonequilibrium phase diagram of the Bose-Hubbard model, Phys. Rev. Lett. **98**, 180601 (2007).

[37] M. Cramer, C. M. Dawson, J. Eisert, and T. J. Osborne, Exact relaxation in a class of nonequilibrium quantum lattice systems, Phys. Rev. Lett. **100**, 030602 (2008).

[38] P. Cai, W. Ruan, Y. Peng, C. Ye, X. Li, Z. Hao, X. Zhou, D.-H. Lee, and Y. Wang, Visualizing the evolution from the Mott insulator to a charge-ordered insulator in lightly doped cuprates, Nat. Phys. **12**, 1047 (2016).

[39] T. Hanaguri, C. Lupien, Y. Kohsaka, D.-H. Lee, M. Azuma, M. Takano, H. Takagi, and J. C. Davis, A 'checkerboard' electronic crystal state in lightly hole-doped $Ca_{2-x}Na_xCuO_2Cl_2$, Nature (London) **430**, 1001 (2004).

[40] C. V. Parker, P. Aynajian, E. H. da Silva Neto, A. Pushp, S. Ono, J. Wen, Z. Xu, G. Gu, and A. Yazdani, Fluctuating stripes at the onset of the pseudogap in the high-T_c superconductor $Bi_2Sr_2CaCu_2O_{8+x}$, Nature (London) **468**, 677 (2010).

[41] K. Fujita, A. R. Schmidt, E.-A. Kim, M. J. Lawler, D. Hai Lee, J. C. Davis, H. Eisaki, and S.-I. Uchida, Spectroscopic imaging scanning tunneling microscopy studies of electronic structure in the superconducting and pseudogap phases of cuprate high-T_c superconductors, J. Phys. Soc. Jpn. **81**, 011005 (2012).

[42] A. Sinha and A. Wietek, Forestalled phase separation as the precursor to stripe order, arXiv:2411.15158.

[43] W. Kadow, L. Vanderstraeten, and M. Knap, Hole spectral function of a chiral spin liquid in the triangular lattice Hubbard model, Phys. Rev. B **106**, 094417 (2022).

[44] I. Ichinose and T. Matsui, Dynamics of holes and spins in the Hubbard *t*-*J* model and high-temperature superconductivity, Phys. Rev. B **45**, 9976 (1992).

[45] A. Bohrdt, F. Grusdt, and M. Knap, Dynamical formation of a magnetic polaron in a two-dimensional quantum antiferromagnet, New J. Phys. **22**, 123023 (2020).

[46] G. Ji, M. Xu, L. H. Kendrick, C. S. Chiu, J. C. Brüggenjürgen, D. Greif, A. Bohrdt, F. Grusdt, E. Demler, M. Lebrat *et al.*, Coupling a mobile hole to an antiferromagnetic spin background: Transient dynamics of a magnetic polaron, Phys. Rev. X **11**, 021022 (2021).

[47] J. Koepsell, J. Vijayan, P. Sompet, F. Grusdt, T. A. Hilker, E. Demler, G. Salomon, I. Bloch, and C. Gross, Imaging magnetic polarons in the doped Fermi-Hubbard model, Nature (London) **572**, 358 (2019).

[48] A. Kale, J. H. Huhn, M. Xu, L. H. Kendrick, M. Lebrat, C. Chiu, G. Ji, F. Grusdt, A. Bohrdt, and M. Greiner, Schrieffer-Wolff transformations for experiments: Dynamically suppressing virtual doublon-hole excitations in a Fermi-Hubbard simulator, Phys. Rev. A **106**, 012428 (2022).

[49] M. Pretko, X. Chen, and Y. You, Fracton phases of matter, Int. J. Mod. Phys. A **35**, 2030003 (2020).

[50] J. Sous and M. Pretko, Fractons from frustration in hole-doped antiferromagnets, npj Quantum Mater. **5**, 81 (2020).

[51] J. Sous and M. Pretko, Fractons from polarons, Phys. Rev. B **102**, 214437 (2020).

[52] S. Sanyal, A. Wietek, and J. Sous, Unidirectional subsystem symmetry in a hole-doped honeycomb-lattice Ising magnet, Phys. Rev. Lett. **132**, 016701 (2024).

[53] S. Jiang, D. J. Scalapino, and S. R. White, Ground-state phase diagram of the t-t'-J model, Proc. Natl. Acad. Sci. USA **118**, e2109978118 (2021).

[54] X. Lu, F. Chen, W. Zhu, D. N. Sheng, and S.-S. Gong, Emergent superconductivity and competing charge orders in hole-doped square-lattice t-J model, Phys. Rev. Lett. **132**, 066002 (2024).

[55] X. Lu, J.-X. Zhang, S.-S. Gong, D. N. Sheng, and Z.-Y. Weng, Sign structure of the t-t'-J model and its physical consequences, Phys. Rev. B **110**, 165127 (2024).

[56] R. B. Sidje, Expokit: A software package for computing matrix exponentials, ACM Trans. Math. Softw. **24**, 130 (1998).

[57] J. Haegeman, J. I. Cirac, T. J. Osborne, I. Pižorn, H. Verschelde, and F. Verstraete, Time-dependent variational principle for quantum lattices, Phys. Rev. Lett. **107**, 070601 (2011).

[58] J. Haegeman, C. Lubich, I. Oseledets, B. Vandereycken, and F. Verstraete, Unifying time evolution and optimization with matrix product states, Phys. Rev. B **94**, 165116 (2016).

[59] D. Poilblanc and T. M. Rice, Charged solitons in the Hartree-Fock approximation to the large-U Hubbard model, Phys. Rev. B **39**, 9749 (1989).

[60] K. Machida, Magnetism in La_2CuO_4 based compounds, Physica C **158**, 192 (1989).

[61] M. Kato, K. Machida, H. Nakanishi, and M. Fujita, Soliton lattice modulation of incommensurate spin density wave in two dimensional Hubbard model—A mean field study, J. Phys. Soc. Jpn. **59**, 1047 (1990).

[62] Y. Nagaoka, Ferromagnetism in a narrow, almost half-filled s band, Phys. Rev. **147**, 392 (1966).

[63] W. Kadow, H.-K. Jin, J. Knolle, and M. Knap, Single-hole spectra of Kitaev spin liquids: From dynamical Nagaoka ferromagnetism to spin-hole fractionalization, npj Quantum Mater. **9**, 32 (2024).

[64] H.-K. Jin, W. Kadow, M. Knap, and J. Knolle, Kinetic ferromagnetism and topological magnons of the hole-doped Kitaev spin liquid, npj Quantum Mater. **9**, 65 (2024).

[65] T. Chalopin, P. Bojović, S. Wang, T. Franz, A. Sinha, Z. Wang, D. Bourgund, J. Obermeyer, F. Grusdt, A. Bohrdt *et al.*, Probing the magnetic origin of the pseudogap using a Fermi-Hubbard quantum simulator, arXiv:2412.17801.

[66] M. Xu, L. H. Kendrick, A. Kale, Y. Gang, C. Feng, S. Zhang, A. W. Young, M. Lebrat, and M. Greiner, A neutral-atom Hubbard quantum simulator in the cryogenic regime, arXiv:2502.00095.

[67] A. Wietek, Xdiag: A high-performance exact diagonalization library, https://github.com/awietek/xdiag.

[68] M. Fishman, S. R. White, and E. M. Stoudenmire, The ITensor software library for tensor network calculations, SciPost Phys. Codebases4 (2022).

[69] M. Fishman, S. R. White, and E. M. Stoudenmire, Codebase release 0.3 for ITensor, SciPost Phys. Codebases4 (2022).